Mathematical Biosciences 387 (2025) 109480

Contents lists available at ScienceDirect

Mathematical Biosciences

journal homepage: www.elsevier.com/locate/mbs

Original Research Article

Recurrent patterns of disease spread post the acute phase of a pandemic: Insights from a coupled system of a differential equation for disease transmission and a delayed algebraic equation for behavioral adaptation

Tianyu Cheng, Jianhong Wu *

Laboratory for Industrial and Applied Mathematics, Department of Mathematics and Statistics, York University, Toronto, Ontario, M3J 1P3, Canada

ARTICLE INFO

MSC:
35K57
34K18
92A15
37N25
35B40
34A09

Keywords:
Behavioral adaptation
Delay-differential–algebraic equations
Hopf bifurcation
Periodic resurgence

ABSTRACT

We introduce a coupled system of a disease transmission differential equation and a behavioral adaptation algebraic renewal equation to understand the mechanisms of nonlinear oscillations post-acute phase of a pandemic. This extends the Zhang–Scarabel–Murty–Wu model, which was formulated and analyzed to describe multi-wave patterns observed at the early stage during the acute phase of the COVID-19 pandemic. Our extension involves the depletion of susceptible population due to infection and contains a nonlinear disease transmission term to reflect the recovery and temporal immunity in the infected population past the acute phase of the pandemic. Examining whether and how incorporating this depletion of susceptible population impacts interwoven disease transmission dynamics and behavioral adaptation is the objective of our current research. We introduce some prototypical risk aversion functions to characterize behavioral responses to perceived risks and show how the risk aversion behaviors and the logistic delay in implementation of behavioral adaptation combined contribute to a dynamic equilibrium state described by a periodic oscillatory wave. We also link the period between two consecutive peaks to basic epidemic parameters, the community flexibility to behavioral change, and the population's tolerance to perceived risks.

1. Introduction

In an early study by Zhang, Scarabel, Murty and Wu [1], it was shown that individual behavioral change in response to perceived infection risks coupled with delay in surveillance, decision-making, and logistic implementation could have contributed to the widely observed oscillatory patterns of infection curves (multi-waves) during the early (acute) phase of the COVID-19 pandemic even when population immunity was not established and the seasonal variation was ruled out. Our objective in the current study is to expand this *outbreak* model (the model that addresses the acute phase of the pandemic) to the post-acute phase of the pandemic and to examine the impact of behavioral adaptation and response delay on the patterns of endemicity when the COVID-19 pandemic becomes *endemic*.

As evidenced by new waves of COVID-19 infection registered in the Americas, Europe, and the Western Pacific in 2024 (see, [2–4]), even after achieving herd immunity following global outbreaks, COVID-19 can resurge regionally and periodically. The WHO did warn about a concerning resurgence of COVID-19 in the summer of 2024 [2,3] due to changes in human behavior such as the relaxation of public health measures, compliance erosion, increment of social interactions, and overconfidence after vaccination. A key question is whether the endemic will be seasonal, i.e. whether it will have predictable fluctuations or patterns that recur or repeat over a certain period. Another important question is whether the COVID-19 resurgence coincides, should COVID-19 become seasonal with the respiration infection seasons, and what will influence the *inter-peak frequency* and magnitude of future COVID-19 endemic waves. Addressing these questions is important for public health policy and vaccination strategies [5].

Taking into account the behavioral adaptation in describing the endemicity post the acute phase requires the incorporation of the immunity of the population. The Zhang–Scarabel–Murty–Wu model [1] is governed by the following delay-algebraic system

$$\begin{cases} I' = \beta(t)I(t) - rI(t), \\ \beta(t) = \dfrac{\beta_c}{1+\kappa\beta(t-\tau)I(t-\tau)}, \end{cases} \tag{1.1}$$

where the susceptible population was assumed to be relatively constant. This was the case in the early phase of the pandemic when immunity was not established in the population. The Zhang–Scarabel–Murty–Wu

* Corresponding author.
E-mail addresses: tianyu45@yorku.ca (T. Cheng), wujh@yorku.ca (J. Wu).

https://doi.org/10.1016/j.mbs.2025.109480
Received 18 December 2024; Received in revised form 4 March 2025; Accepted 23 May 2025
Available online 21 June 2025

model was designed to link the widely observed multiple waves during the early phase of the COVID-19 pandemic to the elasticity/plasticity/flexibility of the effective contact of population disease transmission (characterized by the parameter κ) in response to perceived infection risks and the delay (τ) in logistically implementing the desired adaptation. In their analysis, the basic reproduction number $R_0^c := \beta_c/r$, independent of the behavioral adaptation κ, is assumed to be larger than 1 and hence an outbreak is unavoidable, but the behavioral adaptation may lead to a unique positive equilibrium state

$$\beta_z^* := r,\ I_z^* := \frac{R_0^c - 1}{\kappa r}, \tag{1.2}$$

where the behavioral adaptation equilibrium state is reached when the effective reproduction number β_z/r is the unity, but the equilibrium state of the infection is determined by the plasticity of the population in response to the perceived risks. It is shown in [1] that this positive equilibrium state is destabilized when the lag τ exceeds some critical value, leading to oscillatory patterns as widely reported. The agreement of their simulated amplitudes and inter-wave periods using an appropriately parameterized model with reported data for the first two waves in the study region provides a certain degree of validation to this mechanistic approach. Implicitly assumed in model [1] is that the incidence is directly proportional to the number of infections through the infection transmission effective contact $\beta(t)$, and the total number of susceptible populations remains unchanged. This is a reasonable assumption during the acute phase of a pandemic. This assumption is no longer valid during the endemic phase; replacing this assumption to incorporate the depletion of susceptibles due to infection and the recovery of the susceptibles due to recovery and immunity naturally leads to additional nonlinearity in the model system. Examining whether and how relaxing this assumption impacts interwoven disease transmission dynamics and behavioral adaptation is the objective of our current research.

The rest of the paper will be organized as follows. We will introduce the model formulation and some prototypes of behavior adaptation functions in Section 2 and then present our stability and Hopf bifurcation analysis in Section 3. The general results will be illustrated in Section 4 with numerical illustrations using parameters relevant to the COVID-19 pandemic. We will conclude with some discussions of our results, situating our work compared with the existing literature on epidemic modeling that incorporates behavioral changes in the final section.

2. Interwoven disease transmission and behavioral adaptation

Since we are interested in the impact of behavioral changes and logistic implementation delay post the acute phase of a pandemic (in the situation when the disease becomes an endemic), we can no longer assume that the susceptible population remains relatively unchanged. Rather, we consider a simple SIS framework where infected individuals recover and return to the susceptible class in a closed environment; that is, no demographic birth and death are considered, and no migration is considered. Therefore, the sum of susceptible and infected individuals is a constant N, and the susceptible population at time t is given by $N - I(t)$, with $I(t)$ being the number of infected/infectious individuals.

As the number of susceptible individuals changes post the acute phase, we will use the frequency-dependent transmission mode $\beta I(t)/N$, the so-called standard incidence [6]. Consequently, our baseline coupled disease transmission and behavioral adaptation dynamics is governed by the following delay-algebraic system with logistic nonlinearity:

$$\begin{cases} I'(t) = \beta(t)[N - I(t)]\dfrac{I(t)}{N} - rI(t), \\ \beta(t) = f(\beta(t-\tau), I(t-\tau)), \end{cases} \tag{2.3}$$

where $\beta(t)/N$ is the average daily number of contacts leading to effective disease transmission (the number of contacts times the probability of infection per contact), and r is the recovery rate, which is assumed to be a constant. With this formulation, the function

$$B(t) := \beta(t)(N - I(t))\frac{I(t)}{N}$$

is the daily *incidence*, the number of newly infected cases per unit of time (day) [7].

Perceived Risk: The perceived risk by the population and the decision makers is proportional to the incidence function $B(t)$, but perhaps with a delay ω. In particular, the perceived risk may not be directly proportional to the daily incidence (of infections), but perhaps the daily incidence of hospitalization, ICU admission, or even disease-induced death, resulting in

$$\text{perceived risk}(t) \sim \rho_j B(t - \omega_j),$$

where $j = h, ICU, d$, and ρ_j is the proportion of hospitalization, ICU admission, or disease-induced death of infected individuals, and ω_j is the delay from exposure to infection until hospitalization, ICU admission, and disease-induced death, respectively (including the delay until the information becomes public information).

As the perceived risk of severity of the disease increases, individual behaviors change, and public health policy is developed and implemented for systematic interventions to reduce disease transmission, leading to a decrease of transmission-effective contact. This suggests a qualitative relation between perceived risk $\rho_j B(t - \omega_j)$ as follows

$$\beta(t) \sim \text{ a decreasing function of } \rho_j B(t - \omega_j - \omega_s)$$

with ω_s being the delay in implementing behavioral changes or systematic interventions. In summary, we have the following *behavioral adaptation dynamics*:

$$\beta(t) = F(\rho_j B(t - \tau))$$

with $\tau = \omega_j + \omega_s$.

We now formally define the behavioral adaptation function F:

Definition 2.1. A C^1-smooth function $F : [0, \infty) \to [0, \infty)$ is called a behavioral adaptation function if

(i) (Scaling by plasticity): $F(\xi) := G(\kappa\xi)$, where $\kappa > 0$ is a constant;
(ii) (Monotonicity): $G(x) > 0$ is continuously differentiable and strictly decreasing as a function of $x \geq 0$;
(iii) (Minimal activity and finite jump): $G(\infty) \geq 0$ and $|G'(x)| < C_g$ for all $x \geq 0$, where $C_g > 0$ is a constant.

Remark 2.2. As discussed in [1], the scaling constant $\kappa > 0$ is used as the *flexibility* index to describe the elasticity/flexibility with which the population adapts the behavior in response to the perceived risk. Different populations may have different tolerance to the perceived risks and thus may have different flexibility indices. Here, the perceived risk is proportional to the incidence $x(N-y)y/N$ with $x = \beta$, $S = N - y$ and $y = I$. The disease transmission effective contact per unit time is $F(0)$ when the infection level is small. Therefore, the basic reproduction number is

$$R_0 = F(0)/r,$$

which is independent of the flexibility index κ. Also, note that if we define $\beta_c := \max\{G(\xi)\} = G(0) = F(0) > 0$, then β_c gives the maximal disease transmission effective contact per unit time.

We list three functions that satisfy the aforementioned conditions for a behavioral adaptation function:

1. **Type A**: $F(\xi) = G_A(\kappa\xi)$ with $G_A(\xi) = \frac{\beta_c}{1+\xi}$ [1];
2. **Type B**: $F(\xi) = G_B(\kappa\xi)$ with $G_B(\xi) = \beta_c e^{-\xi}$;
3. **Type C**: $F(\xi) = G_C(\kappa\xi)$ with $G_C(\xi) = \frac{\beta_c(1+e^{-a})}{1+e^{\xi-a}}$ [1] with $a > 0$ being a gain parameter.

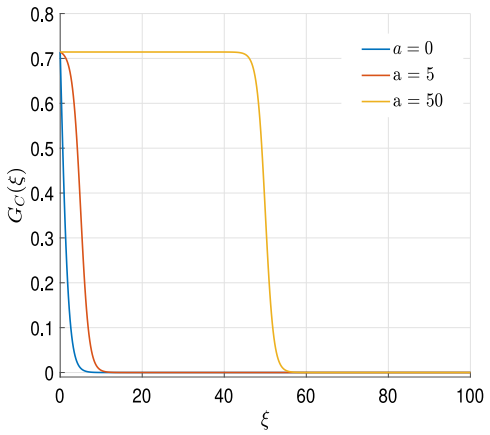

Fig. 1. Illustration of the switching property of the function $G_C(\xi)$ with $a = 0, 5, 50$: When a is relatively large (e.g. $a = 50$), the function $G_C(\xi)$ switches rapidly from the maximum to the minimum.

Remark 2.3. There are many plausible choices of behavioral adaptation functions.

(i) For a given community, the corresponding behavioral adaptation function may be informed by deep learning from disease surveillance data and contact and mobility data during a particular season coupled with symbolic regression analysis (see [8,9] for some recent developments). It is hoped that the interdisciplinary collaboration involving behavioral scientists can help establish a few prototype behavioral functions so real-time data can be used to parameterize these functions to inform the population's perceived risks and behavioral changes.

(ii) Much of the current study is independent of the specific choice of behavioral functions. We will use Type A and Type B as examples to illustrate the qualitative scenarios of the transmission and adaptation dynamics interaction. Type A describes a gradual linear decrease, while Type B describes an exponential decrease. The meaning of the elasticity index κ should be linked to the "perceived risks" discussed early. For example, if the perceived risk is proportional to the number of ICU beds used by the infected individuals due to the disease, i.e., perceived risk$(t) \sim \rho_j B(t - \omega_j)$, then κ is linked to half-effective contact by $\frac{1}{2} = \frac{1}{1+\kappa\rho_{ICU}}$. Therefore, if the rate of ICU usage of infected individuals is 0.1%, then $1 + 0.001\kappa = 2$, i.e., $\kappa = 1000$.

(iii) Should a systematic intervention be implemented in response to the collective desire of the population to adapt behavior, the reduction of the effective transmission contact is more of a switching pattern, represented by $F(\xi) = G_C(\kappa\xi)$ with $G_C(\xi) = \frac{\beta_c(1+e^{-a})}{1+e^{\xi-a}}$ with $a > 0$ as the gain parameter, where the switch will be sharp when the gain parameter a is large; see Fig. 1. We note that $\frac{\partial G_C(\xi)}{\partial a} > 0$ for all $\xi > 0$ and $\lim_{a\to\infty} G_C(\xi) = \beta_c$. Fig. 1 shows that when $\xi \ll a$, the numerator $\beta_c(1+e^{-a})$ of $G_C(\xi)$ dominates, leading to $G_C(\xi) \approx \beta_c$; however, when $\xi > a$, the term $e^{\xi-a}$ dominates, yielding $G_C(\xi)$ decrease rapidly as ξ increase and approach to 0 when $\xi \to \infty$.

We start our qualitative analysis with a result about the positive invariance of the set of epidemiologically plausible initial states in the following phase space:

$$X := \{(\phi, \psi) \in C([-\tau, 0] \to R^2); \phi(s) \in (0, N], \psi(s) > 0 \text{ for all } s \in [-\tau, 0]\}.$$

Proposition 2.4. *The solution $(I(t), \beta(t))$ of the system (2.3) with initial condition $(I, \beta) \in X$ satisfies*

$$(I(t), \beta(t)) \in \Gamma := \{(I(t), \beta(t)) | 0 < I(t) \le N, 0 < \beta(t) < F(0) \quad \text{for any } t > 0\}. \tag{2.4}$$

Proof. The solution $(I(t), \beta(t))$ can be constructed successively in the intervals $[n\tau, (n+1)\tau]$ with $n = 0, 1, \ldots$, and from the construction we can see that both $I(t)$ and $\beta(t)$ are positive for all $t \ge 0$. Furthermore, $\beta(t) \le F(0)$ holds for all $t \ge 0$ due to property of $F(x)$. To prove that $I(t) \le N$ for all $t \ge 0$, all we need to see is that if there were the first $T > 0$ such that $I(T) = N$, then $I'(T) < -rN < 0$. □

Obviously, $E_0 = (\beta_0, I_0) = (F(0), 0)$ is always an equilibrium of (2.3). If $R_0 < 1$, then using the inequality that $I(t) \le I(0)\exp(r(R_0-1)t)$ for any $t \ge 0$, we have $I(\infty) = 0$ and $\beta(\infty) = F(0)$. We conclude that if $R_0 < 1$, then system (2.3) has a unique equilibrium $E_0 = (F(0), 0)$, which is globally attractive.

To prepare for the next step of qualitative analysis of the model system, we explore some properties of $f(x, y)$ on $(x, y) \in [0, \infty) \times [0, N]$ according to the baseline assumptions about the behavioral adaptation function. Taking the partial derivatives of $f(x, y)$ with respect to x, y, we obtain

$$\begin{aligned} f'_x(x, y) &:= \frac{\partial f(x, y)}{\partial x} = F'(x(N - y)y/N)(N - y)y/N, \\ f'_y(x, y) &:= \frac{\partial f(x, y)}{\partial y} = F'(x(N - y)y/N)x(N - 2y)/N. \end{aligned} \tag{2.5}$$

The following result follows from the assumption that $F'(\xi) < 0$ for all $\xi \ge 0$:

Proposition 2.5 (*Behavioral Feedback Properties*). *We have the feedback properties of the behavioral adaptation and infection level on the change of incidence:*

(i) The behavioral adaptation feedback for incidence is positive: $f'_x(x, y) \le 0$ for any $(x, y) \in [0, \infty) \times [0, N]$;

(ii) The critical level of the current level of infection on incidence: $f'_y(x, y) \ge 0$ if and only if $y \ge N/2$.

3. Endemicity scenarios of disease transmission and behavioral adaptation

The endemic equilibrium (EE) $E^* = (\beta^*, I^*)$ is given by the intersection of the following two curves

$$l_1 : y = F(rx), \; l_2 : y = \frac{rN}{N - x}.$$

Thus, if $E^* = (\beta^*, I^*)$ exists, it must satisfy

$$\beta^* = F(rI^*), \; \beta^* = \frac{rN}{N - I^*}. \tag{3.6}$$

Lemma 3.1. *The following existence, uniqueness of endemic equilibrium, and its dependence on the behavioral adaptation elasticity index κ hold:*

(i) If and only if $R_0 := F(0)r^{-1} > 1$, can an endemic equilibrium $I^* \in (0, N)$ exist and this equilibrium is unique;

(ii) When $R_0 > 1$, the I^* component of the endemic equilibrium is a decreasing function of the behavioral adaptation index κ.

Proof. We note that F is a decreasing function, and $1/(N - y)$ is an unbounded increasing function of $y \in [0, N)$. The results follow. □

From the critical level of the current level of infection on incidence, we note that $N/2$ is a critical threshold for the sign of $f'_I(\beta^*, I^*)$, which is important for our Hopf bifurcation analysis later.

Lemma 3.2. *$I^* \le N/2$ if and only if*

$$\kappa \ge \kappa_c := 2G^{-1}(2r)r^{-1}N^{-1}.$$

Proof. The result follows from the analytic expression for calculating the I^* component. □

We now describe the impact of the gain parameter on endemic states for the switching function **Type C**.

Lemma 3.3 (*Impact of the Gain Parameter on Endemic States*). *For the* **Type C**, *the gain parameter a has no impact on R_0, but it influences the endemic state. The I^* component of the endemic equilibrium is an increasing function of gain parameter a; $\beta^* = \beta^*(a)$, $I^* = I^*(a)$. With these notations, we have $\beta^*(\infty) = \beta_c$ and $I^*(\infty) = N(1 - R_0^{-1})$.*

Proof. First of all, we note that as $a \to \infty$, $I^* = N(1-R_0^{-1})$ and $\beta^* = \beta_0$ hold. Taking a derivative of $F(rI^*) = \frac{rN}{N-I^*}$ with respect to the gain parameter a on both sides, we have

$$\frac{\partial F(rI^*)}{\partial a} + \frac{\partial F(rI^*)}{\partial I^*}\frac{\partial I^*}{\partial a} = \frac{rN}{(N-I^*)^2}\frac{\partial I^*}{\partial a},$$

that is,

$$\frac{\partial G(\kappa r I^*)}{\partial a} = \left(- \frac{\partial G(\kappa r x)}{\partial x}\bigg|_{x=I^*} + \frac{rN}{(N-I^*)^2} \right) \frac{\partial I^*}{\partial a}.$$

Since

$$\frac{\partial G(\kappa r I^*)}{\partial a} > 0, \quad \frac{\partial G(\kappa r x)}{\partial x}\bigg|_{x=I^*} < 0,$$

we have $\frac{\partial I^*}{\partial a} > 0$. The conclusion follows. □

We use Fig. 2-(a,b,c) to illustrate the dependence of the behavioral adaptation on the index κ and illustrate the intersection of the behavioral adaptation and the ratio of the total populations over the total number of infections when $\beta_c > r$ (i.e., $R_0 > 1$). When N is fixed to 5×10^3, as κ increases, the behavioral response decreases, and the I^* of the endemic equilibrium decreases. When κ increases to pass $\kappa_c = R_0/(Nr)^{-1}$, $I^* = N/2$. In particular, in Fig. 2-(a), we observed that when $\kappa = R_0/(Nr)^{-1} = 2.1953 \times 10^{-3} > \kappa_c$, $I^* = 1607.17 < N/2$. Fig. 2-(d) illustrates the dependence of I^* and β^* on the gain parameter.

We now proceed to the study of transmission dynamics and behavioral adaptation near E^*. The linearization at (β^*, I^*) of (2.3) is

$$\begin{cases} I' = \frac{rI^*}{\beta^*}\beta - (\beta^* I^*/N)I, \\ \beta(t) = f'_\beta(\beta^*, I^*)\beta(t-\tau) + f'_I(\beta^*, I^*)I(t-\tau). \end{cases} \tag{3.7}$$

Submitting $I = e^{\lambda t}\hat{I}$ and $\beta = e^{\lambda t}\hat{\beta}$ leads to

$$\begin{cases} \lambda \hat{I} = \frac{rI^*}{\beta^*}\hat{\beta} - (\beta^* I^*/N)\hat{I} \\ \hat{\beta}(1 - f'_\beta(\beta^*, I^*)e^{-\lambda\tau}) = \left(f'_I(\beta^*, I^*)\hat{I}\right) e^{-\lambda\tau}. \end{cases} \tag{3.8}$$

where $(\hat{\beta}, \hat{I})$ is the initial value. So the characteristic equation of (3.7) is

$$\Delta(\lambda, \tau) := f_2(\lambda) + f_1(\lambda)e^{-\lambda\tau}, \tag{3.9}$$

where

$$\begin{aligned} f_1(\lambda) &= -\left(\left(\beta^*\lambda + (\beta^*)^2 I^*/N\right) f'_\beta(\beta^*, I^*) + r f'_I(\beta^*, I^*) I^* \right), \\ f_2(\lambda) &= \beta^*(\lambda + \beta^* I^*/N). \end{aligned} \tag{3.10}$$

From (3.9), $\lambda = 0$ is not an eigenvalue. When $\tau = 0$, the eigenvalue is

$$\lambda_0 = \frac{L_1}{1 - f'_\beta(\beta^*, I^*)} \frac{I^*}{\beta^* N},$$

where

$$\begin{aligned} L_1 &:= rN f'_I(\beta^*, I^*) + (f'_\beta(\beta^*, I^*) - 1)\beta^{*2} \\ &= rN F'(\beta^*(N-I^*)I^*/N)\beta^*(N-2I^*)/N \\ &\quad + (F'(\beta^*(N-I^*)I^*/N)(N-I^*)I^*/N - 1)\beta^{*2} \\ &= rF'(rI^*)\beta^*(N-2I^*) + (F'(rI^*)rI^*/\beta^* - 1)\beta^{*2} \\ &= (rF'(rI^*)(N-2I^*) + F'(rI^*)rI^* - \beta^*)\beta^* \\ &= \left(rF'(rI^*)(N-I^*) - \beta^*\right)\beta^* < 0. \end{aligned} \tag{3.11}$$

Then $\lambda_0 < 0$ since $L_1 < 0$ and $f'_\beta(\beta^*, I^*) < 0$. Therefore, we have the following

Theorem 3.4. *When $R_0 > 1$, system (2.3) has a unique positive equilibrium $E^* = (\beta^*, I^*)$ satisfying (3.6). When $\tau = 0$, the endemic equilibrium E^* is locally stable.*

This theorem shows that if the perceived risk is proportional to the daily incidence and the perceived risk induces behavioral adaptation immediately, the system will reach and remain at the endemic equilibrium state. To understand the impact of response delay on the interaction of transmission and behavior dynamics, we now conduct a local Hopf bifurcation analysis using τ as a parameter. In what follows, we will assume

$$L_c := 1 + f'_\beta(\beta^*, I^*) > 0. \tag{3.12}$$

This assumption is related to excluding the periodic-doubling bifurcation of the algebraic component of the coupled system. We will revisit this assumption later.

To consider when the endemic equilibrium will lose its stability by increasing the delay τ, we consider the situation when the characteristic equation will have a pair of purely imaginary zeros: $\lambda = \pm\omega i$. Substituting this into (3.9) gives

$$A_1 + iA_2 = 0, \tag{3.13}$$

where

$$\begin{aligned} A_1 &= g_2(\omega)\sin(\omega\tau) + g_1\cos(\omega\tau) - I^*\beta^{*2}/N, \\ A_2 &= g_2(\omega)\cos(\omega\tau) - g_1\sin(\omega\tau) - \beta^*\omega \end{aligned} \tag{3.14}$$

with

$$g_1 = (\beta^{*2} f'_\beta(\beta^*, I^*)/N + r f'_I(\beta^*, I^*))I^*, \quad g_2(\omega) = \beta^*\omega f'_\beta(\beta^*, I^*) < 0. \tag{3.15}$$

Taking square of $A_1 + I^*\beta^{*2}/N$ and $A_2 + \beta^*\omega$, we conclude that $x = \omega^2$ must be given by

$$\beta^{*2}(f'_\beta(\beta^*, I^*)^2 - 1)x + ((\beta^{*2} f'_\beta(\beta^*, I^*) + r f'_I(\beta^*, I^*))^2 - \beta^{*4})I^{*2} = 0. \tag{3.16}$$

On the other hand, we know that Eq. (3.16) has a unique root given by

$$x_* := \frac{L_2 L_1}{L_c} \frac{I^{*2}}{(1 - f'_\beta(\beta^*, I^*))N^2\beta^{*2}}, \tag{3.17}$$

with L_c is given in (3.12).

$x_* > 0$ if and only if $L_2 < 0$, where L_2 is defined as

$$\begin{aligned} L_2 &:= rN f'_I(\beta^*, I^*) + (f'_\beta(\beta^*, I^*) + 1)\beta^{*2} \\ &= \left(rF'(rI^*)(N-I^*) + \beta^*\right)\beta^*, \\ &= \left(F'(rI^*)(N-I^*)^2 + N\right)\frac{r\beta^*}{N-I^*}. \end{aligned} \tag{3.18}$$

Hence, if $L_2 < 0$, then $\pm\sqrt{x_*}i$ is the pure imaginary roots of the characteristic Eq. (3.9) and $g_1 < -\beta^{*2} I < 0$. Denote $\omega_0 := \sqrt{x_*}$. We now use the equations $A_1 = 0$ and $A_2 = 0$ to get

$$\begin{cases} \cos(\omega_0\tau) = \dfrac{\beta^*(g_1 I^*\beta^* + N g_2(\omega_0)\omega_0)}{N(g_1^2 + g_2(\omega_0)^2)} < 0, \\ \sin(\omega_0\tau) = -\dfrac{\beta^*(-g_2(\omega_0)I^*\beta^* + N g_1\omega_0)}{N(g_1^2 + g_2(\omega_0)^2)} > 0. \end{cases} \tag{3.19}$$

We note also that $L_2 < 0$ ensures the existence of a unique $\theta \in (0, \pi/2)$ such that

$$\theta = \arctan\left(\frac{N - 2I^*}{2I^*}\right). \tag{3.20}$$

In what follows, we denote by

$$q_M := \frac{2\pi}{\pi - \theta}, \tag{3.21}$$

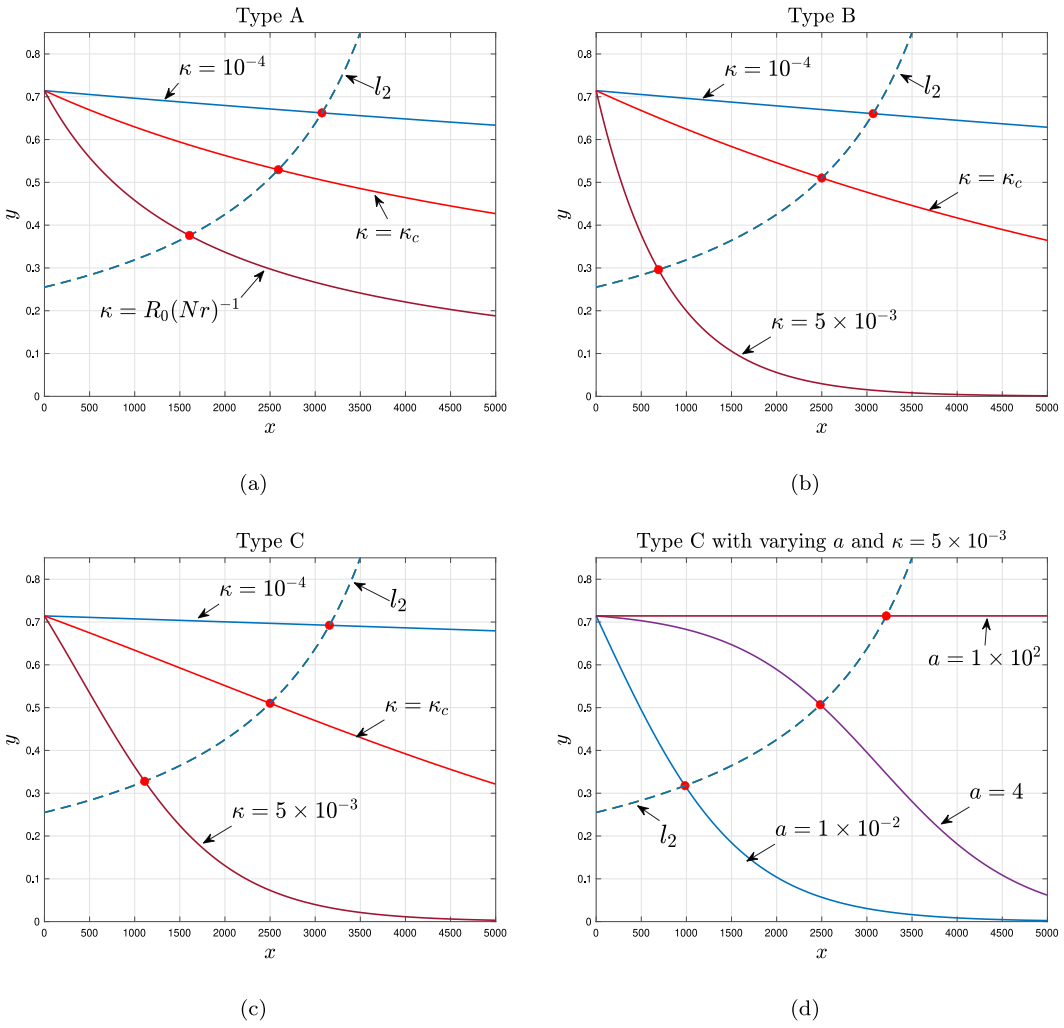

Fig. 2. Illustrations of the curves l_1 and l_2: l_1 with different κ in solid lines, l_2 in a dash line. The red curve corresponds to l_1 at the critical value $\kappa = \kappa_c$. The parameters value are $N = 5 \times 10^3$, $r = 0.2551$, $\beta_c = 0.7143$ so $R_0 = 2.8$. (a). For the **Type A**, $\kappa_c = 6.272 \times 10^{-4}$; (b). For the **Type B**, $\kappa_c = 5.276 \times 10^{-4}$; (c). For the **Type C**, $a = 0.5$, $\kappa_c = 1.133 \times 10^{-3}$; (d). For the **Type C**, when a is very large (e.g., $a = 10^2$), $(\beta^*, I^*) \approx (\beta_c, N(1 - R_0^{-1})) = (0.7143, 3214.3)$.

and note that $q_M \in (2,4)$.

Since

$$\tan(\omega_0\tau) = -\frac{N^2 I^* f_I'(\beta^*, I^*) r\omega_0}{\beta^*(rI^{*2} N f_I'(\beta^*, I^*) + (\beta^{*2} I^{*2} + N^2\omega_0^2) f_\beta'(\beta^*, I^*))} < 0$$

we have

$$\omega_0\tau_0 = \pi + \arctan\left(-\frac{N^2 I^* f_I'(\beta^*, I^*) r\omega_0}{\beta^*(rI^{*2} N f_I'(\beta^*, I^*) + (\beta^{*2} I^{*2} + N^2\omega_0^2) f_\beta'(\beta^*, I^*))}\right) \in (\pi/2, \pi),$$

with

$$\arctan\left(-\frac{N^2 I^* f_I'(\beta^*, I^*) r\omega_0}{\beta^*(rI^{*2} N f_I'(\beta^*, I^*) + (\beta^{*2} I^{*2} + N^2\omega_0^2) f_\beta'(\beta^*, I^*))}\right) \in (-\pi/2, 0).$$

Direct calculations lead to a sequence of solutions $\tau_k, k = 0, 1, \ldots$ of Eq. (3.19) as follows:

$$\begin{aligned}\tau_0 &= \frac{1}{\omega_0}\left(\pi + \arctan\left(-\frac{N^2 I^* f_I'(\beta^*, I^*) r\omega_0}{\beta^*(rI^{*2} N f_I'(\beta^*, I^*) + (\beta^{*2} I^{*2} + N^2\omega_0^2) f_\beta'(\beta^*, I^*))}\right)\right) \\ &> \frac{1}{\omega_0}\left(\pi + \arctan\left(-\frac{N - 2I^*}{2I^*}\right)\right)\end{aligned} \tag{3.22}$$

and

$$\tau_k = \tau_0 + \frac{2k\pi}{\omega_0}, \quad k = 0, 1, 2, \ldots.$$

We note that $\frac{2\pi}{\omega\tau_0} \in (2, q_M) \subseteq (2,4)$ and $\frac{2\pi}{\omega\tau_k} \in (\frac{1}{1/2+k}, \frac{1}{1/q_M+k}) \subseteq (0,1)$ for $k = 1, 2, \ldots$ These are important inequalities to characterize the inter-wave distances of bifurcated oscillatory patterns.

To guarantee the occurrence of a local bifurcation of periodic solutions, we need to verify the transversality condition [10,11]. For this purpose, we obtain from (3.9) that

$$\left(\frac{\mathrm{d}\lambda}{\mathrm{d}\tau}\right)^{-1} = \frac{f_2'(\lambda) - f_1(\lambda)e^{-\lambda\tau}\tau + f_1'(\lambda)e^{-\lambda\tau}}{\lambda f_1(\lambda)e^{-\lambda\tau}} = -\left(\frac{f_2'}{\lambda f_2} + \frac{\tau}{\lambda} - \frac{f_1'(\lambda)}{\lambda f_1(\lambda)}\right). \tag{3.23}$$

Since $L_2 < 0$ and $L_c > 0$ combined implies $f_I'(\beta^*, I^*) < 0$, we have

$$\begin{aligned}&\mathrm{Re}\left(\frac{\mathrm{d}\lambda}{\mathrm{d}\tau}\Big|_{\tau=\tau^n}^{-1}\right) = -\mathrm{Re}\left(\frac{f_2'}{\lambda f_2} - \frac{f_1'}{\lambda f_1}\right) \\ &= \frac{N^3 rI^{*2} f_I'(\beta^*, I^*)(N f_I'(\beta^*, I^*) r + 2\beta^{*2} f_\beta'(\beta^*, I^*))}{(\beta^{*2} I^{*2} + N^2\omega_0^2)((\beta^{*2} f_\beta'(\beta^*, I^*) + N f_I'(\beta^*, I^*) r)^2 I^{*2} + \beta^{*2} f_\beta'(\beta^*, I^*)^2\omega_0^2)} \\ &= \frac{N^3 rI^{*2} f_I'(\beta^*, I^*) rF'(rI^*) N\beta^*}{(\beta^{*2} I^{*2} + N^2\omega_0^2)((\beta^{*2} f_\beta'(\beta^*, I^*) + N f_I'(\beta^*, I^*) r)^2 I^{*2} + \beta^{*2} f_\beta'(\beta^*, I^*)^2\omega_0^2)} > 0.\end{aligned} \tag{3.24}$$

In summary, we established the necessary condition for the existence of purely imaginary eigenvalues, i.e. $L_2 < 0$ and verify the

transversality condition. Consequently, we obtained the following Hopf bifurcation theorem:

Theorem 3.5. *Given that $L_c > 0$ and $R_0 > 1$, we have the following conclusions:*

(i) If $L_2 > 0$, then E^* is locally asymptomatic stable for any $\tau \geq 0$.
(ii) If $L_2 < 0$, then there exists a critical τ_0 given in (3.22) such that when $\tau \in [0, \tau_0)$, all of real parts of eigenvalues are negative and E^* is locally asymptotically stable;
(iii) If $L_2 < 0$, and τ passes through the critical value τ_0 and other $\tau_k, k \geq 0$, there will be local Hopf bifurcations of periodic solutions. More precisely, at each $\tau = \tau_k$, there appears a pair of purely imaginary eigenvalues $\pm\omega_0 i$ with $x_* = \omega_0^2$ given in (3.17). When $\tau \in (\tau_k, \tau_{k+1}]$, there are $k+1$ pairs of eigenvalues with positive real part, so E^* is unstable for $\tau > \tau_0$; system (2.3) undergoes a Hopf bifurcation of periodic solutions at E^* when τ passes through τ_k for each $k = 0, 1, 2, \ldots$. Furthermore, the period T of periodic solutions bifurcate at τ_0 is close to $\frac{2\pi}{\omega_0}$ with $T \in (2\tau_0, q_M \tau_0)$, where $q_M \in (2, 4)$ is given in (3.21).

Proof. (i). From the expression (3.17) of x^*, we see that when $L_2 > 0$, then $x^* < 0$ holds, implying that there is no purely imaginary root of Eq. (3.9) for all $\tau \geq 0$. Thus, no root of Eq. (3.9) crosses the purely imaginary axis in the complex plane from the left half to the right half when τ increases from zero.

(ii) and (iii). From the above arguments, we see that only when $L_2 < 0$, Eq. (3.9) has purely imaginary roots. Since transversality at critical values τ_k holds, i.e.

$$\mathrm{Re}\left(\frac{\mathrm{d}\lambda}{\mathrm{d}\tau}\Big|^{-1}_{\tau=\tau^n}\right) > 0,$$

the crossing at $\pm i\sqrt{x^*}$ is always from left to right when τ increases from 0 and passes all those critical values τ_k, $k = 0, 1, 2, \ldots$. All roots of Eq. (3.9) have negative real parts for $\tau < \tau_0$. and Eq. (3.9) has a pair of roots with positive real parts when τ passes τ_0. □

Using the expressions of L_2 given by (3.18) and L_c given by (3.12), we conclude that

$$L_2 < 0 \text{ implies } f_I'(\beta^*, I^*) < 0 \text{ (i.e. } I^* < N/2 \text{ or } \kappa > \kappa_c)$$

given that $L_c > 0$. Conversely, $I^* > N/2$ ensures $L_2 > 0$. Therefore, we show that the large value of infections (or equivalently, small population flexibility to perceived risk) at the endemic equilibrium is always stable. Namely,

Corollary 3.6. *Given that $R_0 > 1$ and $|f_\beta'(\beta^*, I^*)| < 1$, E^* is locally asymptomatically stable for any $\tau \geq 0$ if $I^* > N/2$ (or equivalently, if $\kappa < \kappa_c$).*

Remark 3.7. The case when $|f_\beta'(\beta^*, I^*)| > 1$ raises technical difficulties, and the above technique is invalid to determine dynamics around E^*. Fig. 8 shows there can exist periodic oscillations even when $|f_\beta'(\beta^*, I^*)| > 1$.

From the expressions in (3.12) and (3.18), whether Hopf bifurcation occurs or not is intrinsically linked to the level of the endemic component I^*, which in turn depends on the behavioral flexibility κ. To derive more explicit conditions through I^*, we now consider some additional properties of the function $G(\xi)$ borrowing from the literature in economics study [12].

Definition 3.8 (*Risk Assertion*)**.** We define the following risk aversion properties for the function G:

(i) G is said to have the property of risk aversion if $G''(\xi) > 0$ for any $\xi > 0$.
(ii) G is said to have the property of relative risk aversion if $\xi G(\xi)$ is a strictly increasing function for $\xi > 0$.

Clearly, G_A exhibits both risk aversion and relative risk reversion and G_B has the property of risk aversion.

Define

$$Q(x) := \kappa G'(\kappa r N x)(1-x)^2 + 1/N \quad \text{for } x \in [0, 1]. \tag{3.25}$$

So we can rewrite (3.18) as $L_2 = Q(I^*/N)\frac{N^2 r\beta^*}{N - I^*}$. We can see that if $G(\xi)$ is risk aversion, then $Q'(x) \geq 0$ for $x \in [0, 1]$. Therefore,

$$\kappa \leq \kappa_l := -1/(NG'(0)) \tag{3.26}$$

implies that $Q(x) \geq 0$ for all $x \in [0, 1]$, and consequently $L_2 > 0$. So, for $L_2 < 0$ we must have $\kappa > \kappa_l$. On the other hand, for $\kappa > \kappa_l$, the fact that $Q(0) = \kappa G'(0) + 1/N < 0$ (since $\gamma > \kappa_l$) $Q(1) = 1/N > 0$ implies that there is a unique threshold $i_g^* \in (0, 1)$ such that $Q(i_g^*) = 0$, and $Q(x) < 0$ if and only if $x < i_g^*$. Note that i_g^* is implicitly dependent on κ, so in what follows we write $i_g^*(\kappa)$. Note also that from Lemma 3.2 it follows that

$$I^*/N \leq i_g^* \text{ if and only if } \kappa \geq G^{-1}\left(r/(1 - i_g^*(\kappa))\right)(rN i_g^*(\kappa))^{-1} := \mathcal{K}_g(\kappa),$$

the second part involves solving an implicit inequality for κ. Thus, we have established the following result, which confirms that $L_2 < 0$ if the behavioral flexibility κ is sufficiently large.

Lemma 3.9. *If G is risk aversion, then condition $L_2 < 0$ is satisfied if $\kappa > \kappa_l$ and $I^*/N < i_g^* < 1$. In other words, $L_2 < 0$ if and only if $\kappa > \max\{\kappa_l, \mathcal{K}_g(\kappa)\}$.*

We now consider the condition $L_c < 0$. Based on (3.6) and the expression of $f_x'(x, y)$ shown in (2.5), we can simplify $f_\beta'(\beta^*, I^*)$ to yield

$$\begin{aligned} f_\beta'(\beta^*, I^*) &= F'(rI^*)(N - I^*)I^*/N = F'(rI^*)rI^*/F(rI^*) \\ &= (\kappa r I^*)G'(\kappa r I^*)/G(\kappa r I^*). \end{aligned} \tag{3.27}$$

It follows that $f_\beta'(\beta^*, I^*) > -1$ is equivalent to $(\kappa r I^*)G'(\kappa r I^*) + G(\kappa r I^*) > 0$. Hence, we can conclude that any relative risk aversion G satisfies $L_c > 0$.

Lemma 3.10. *If G is relative risk revision and $R_0 > 1$, then condition $f_\beta'(\beta^*, I^*) > -1$, i.e., $L_c > 0$.*

4. Comparison between acute phase and post acute phase

In this section, we illustrate all of the technical conditions and our conclusions using **Type A**, **Type B** and **Type C** functions. We also compare the equilibrium value and oscillatory patterns during and post the acute phase of a pandemic.

4.1. Endemic states

For **Type A**, we have

$$G_A''(\xi) = \frac{2\beta_c}{(\xi+1)^3} > 0, \quad (\xi G_A(\xi))' = \frac{\beta_c}{(\xi+1)^2} > 0 \text{ for any } \xi > 0,$$

and

$$f(x, y) = \frac{\beta_c}{1 + \kappa x(N-y)y/N},$$

with

$$f_x'(x, y) = -\frac{\beta_c \kappa (N-y)y/N}{(1 + \kappa x(N-y)y/N)^2} = -\frac{\kappa}{\beta_c}(y/N)(N-y)f(x, y)^2,$$

$$f_y'(x, y) = -\frac{\beta_c \kappa x(N-2y)/N}{(1 + \kappa x(N-y)(y/N))^2} = -\frac{\kappa}{\beta_c}x((N-2y)/N)f(x, y)^2.$$

The reproduction number is $R_0 = \frac{\beta_c}{r}$ like what was observed in [1] for the *outbreak* situation. The EE $E^* = (\beta^*, I^*)$ is given by

$$\beta^* = \frac{\kappa r^2 N + \beta_c}{Nkr + 1}, \ I^* = \frac{R_0 - 1}{\kappa r + R_0/N}. \tag{4.28}$$

Therefore, $|f'_\beta(\beta^*, I^*)| = \frac{\kappa r}{\beta_c}(\beta^* I^*) = \frac{\kappa r}{\beta_c}\frac{\beta_c I^*}{1+\kappa r I^*} < 1$ (i.e. $L_c > 0$). Furthermore, the critical threshold L_2 is given by

$$L_2 = -(\frac{\kappa r^2 N}{\beta_c} - 1)\beta^{*2}. \tag{4.29}$$

The corresponding κ_l defined in (3.26) is $\kappa_l = 1/(\beta_c N)$, and i_g^* is given by

$$i_g^* = \frac{\sqrt{\beta_c \kappa N}\,(N\kappa r + 1) - N\kappa\left(\beta_c + r\right)}{N\kappa\left(N\kappa r^2 - \beta_c\right)} = \frac{(\beta_c \kappa N - 1)}{\sqrt{\beta_c \kappa N}\,(N\kappa r + 1) + N\kappa\left(\beta_c + r\right)}. \tag{4.30}$$

Therefore,

$$\frac{i_g^*}{I^*/N} = \frac{(R_0\kappa r N - 1)(\kappa r N + R_0)}{\left(\sqrt{R_0 \kappa r N}\,(N\kappa r + 1) + N r \kappa\left(R_0 + 1\right)\right)(R_0 - 1)}.$$

This shows that $i_g > I^*/N$ if and only if $\sqrt{R_0 \kappa r N} < \frac{(\kappa r N - 1)R_0}{R_0 - 1}$. The latter is equivalent to $(\kappa N r - 1/R_0)(\kappa r N - R_0) > 0$. This inequality is equivalent to $\kappa r N > R_0$, or $\kappa > \beta_c/(Nr^2)$ if $\kappa > \kappa_l$. Additionally, $\beta_c/(Nr^2) > \kappa_l$ if we assume $R_0 > 1$. It follows directly from (4.29) that $L_2 \le 0$ if and only if

$$\kappa \ge \kappa^* := \beta_c/(Nr^2) = R_0/(rN). \tag{4.31}$$

Further, based on the expression of I^* given in (4.28), the condition $\kappa \ge \kappa^*$ is equivalent to

$$I^*/N < i_{c,1}^* := \frac{1}{2} - \frac{1}{2R_0}. \tag{4.32}$$

Obviously, $i_{c,1}^* < 1/2$ given that $R_0 > 1$. Finally, note that if $R_0 > 1$ then $\kappa_l < \kappa^*$.

From expression of (β^*, I^*) (endemic equilibrium at the post-acute phase) shown in (4.28) and (β_z^*, I_z^*)(equilibrium during the acute phase) given in (1.2), we obtain

$$\frac{I^*}{I_z^*} = \frac{1}{1 + R_0/(\kappa N r)} < 1, \ \beta^* - \beta_z^* = \frac{r(R_0 - 1)}{\kappa N r + 1} > 0,$$

and

$$\lim_{N\to\infty} \beta^* = r = \beta_z^*, \ \lim_{N\to\infty} I^* = \frac{R_0 - 1}{\kappa r} = I_z^*.$$

Summarizing the above discussions about (β^*, I^*) and (β_z^*, I_z^*), we obtain the following result that compares the equilibrium infection and transmission effective contact during the acute and post-acute phase.

Theorem 4.1 (*Comparison of Equilibrium between Acute Phase and Post Acute Phase*). *Fixing parameters β_c, r and κ, we have $\beta^* > \beta_z^*$, $I^* < I_z^*$. That is, at the equilibrium, the transmission effective contact post the acute phase is larger than during the acute phase, and the level of infection is lower during the post-acute phase than during the acute phase. However, when the total population is large, there is no essential difference, i.e., $I^* \approx I_z^*$ and $\beta^* \approx \beta_z^*$ if $N \to \infty$ (see Fig. 3).*

For **Type B**, we have $G_B''(\xi) = \beta_c e^{-\xi} > 0$ for any $\xi \ge 0$. We have also $f(x, y) = \beta_c e^{-\kappa x(N-y)y/N}$, so $f'_x(x, y) = -\kappa(N - y)(y/N)f(x, y)$, $f'_y(x, y) = -\kappa x((N - 2y)/N)f(x, y)$. The reproduction number is $R_0 = \beta_c/r$, and the EE satisfies:

$$\beta^* = \beta_c e^{-\kappa r I^*}, \ \beta^* = \frac{rN}{N - I^*}.$$

We thus conclude $|f'_\beta(\beta^*, I^*)| = \kappa r I^* = \ln(\beta_c/\beta^*)$. This shows that if and only if $\beta_c/e < \beta^*$ (or equivalently, $I^* < 1/(\kappa r)$), $|f'_\beta(\beta^*, I^*)| < 1$ holds. By direct computations, the critical threshold L_2 is given by

$$L_2 = -[\kappa r(N - I^*) - 1]\beta^{*2}. \tag{4.33}$$

Rather than applying Lemma 3.9, we can obtain more directly from (4.33) that $L_2 < 0$ if and only if

$$I^*/N < 1 - \frac{1}{\kappa N r} := i_{c2}^*. \tag{4.34}$$

For **Type C**, we have

$$G'_C(x) = G_C(x)^2\left(\frac{1}{\beta_c(1 + e^{-a})} - \frac{1}{G_C(x)}\right),$$

$$f'_\beta(\beta^*, I^*) = \kappa r I^*\left(\frac{1}{\beta_c(1 + e^{-a})}\beta^* - 1\right),$$

$$L_2 = \beta^*\left(\left(\frac{\kappa r^2 N}{\beta_0(1 + e^{-a})} + 1\right)\beta^* - \kappa r^2 N\right). \tag{4.35}$$

Therefore,

$$L_2 < 0 \text{ if and only if } \beta^* < \frac{\kappa r^2 N}{1 + \frac{\kappa r^2 N}{\beta_c(1+e^{-a})}} \ \left(\text{or, equivalently, } I^* < I_{G_c}^*\right),$$

where

$$I_{G_c}^*(a) := N\left(1 - \frac{1}{(1 + e^{-a})R_0}\right) - \frac{1}{\kappa r} < N, \ \ i_{G_c}^*(a) := I_{G_c}^*(a)/N \tag{4.36}$$

and $I_{G_c}^*(a)$ is a decreasing function of a with

$$I_{G_c}^*(\infty) = N(1 - R_0^{-1}) - (\kappa r)^{-1}, \ \ I_{G_c}^*(0) = N(1 - 0.5R_0^{-1}) - (\kappa r)^{-1}.$$

Combined with Lemma 3.3, we obtain (see Fig. 4 for illustrations):

Lemma 4.2 (*Impact of Gain Parameter on Possibility of Oscillations*). *For* **Type C**, *we have*

(i) When $I_{G_c}^*(0) < I^*(0)$, $L_2 > 0$ holds for any $a \ge 0$;

(ii) When $I_{G_c}^*(\infty) > I^*(\infty)$, $L_2 < 0$ holds for any $a \ge 0$;

(iii) When $I_{G_c}^*(0) > I^*(0)$ and $I_{G_c}^*(\infty) < I^*(\infty)$, there exists a unique critical value a^* such that $L_2 < 0$ if and only if $a \in (0, a^*)$.

Continuing our discussions on **Type C**, we obtain that $f'_\beta(\beta^*, I^*) > -1$ if and only if $h_c(I^*) > 0$, where

$$h_c(x) := \kappa r \beta_c(1 + e^{-a})x^2 - \left(\beta_c(1 + e^{-a})(N\kappa r + 1) - \kappa r^2 N\right)x + N\beta_c(1 + e^{-a}).$$

Denote

$$\begin{aligned}\Delta_C &:= (\beta_c(1 + e^{-a})(N\kappa r + 1) - \kappa r^2 N)^2 - 4(\beta_c(1 + e^{-a}))^2 N\kappa r \\ &= (\beta_c(1 + e^{-a})(\sqrt{N\kappa r} + 1)^2 - \kappa r^2 N)(\beta_c(1 + e^{-a})(\sqrt{N\kappa r} - 1)^2 - \kappa r^2 N).\end{aligned} \tag{4.37}$$

We have

$$\begin{aligned} I_{G_c}^1 &:= \frac{\beta_c(1 + e^{-a})(N\kappa r + 1) - \kappa r^2 N - \sqrt{\Delta_C}}{2\kappa\beta_c(1 + e^{-a})r}, \\ I_{G_c}^2 &:= \frac{\beta_c(1 + e^{-a})(N\kappa r + 1) - \kappa r^2 N + \sqrt{\Delta_C}}{2\kappa\beta_c(1 + e^{-a})r}. \end{aligned} \tag{4.38}$$

Since $R_0 > 1$, we obtain $\left(\kappa r N + 1 - \frac{\kappa r N}{R_0(1+e^{-a})}\right) > 0$, and $\beta_c(1 + e^{-a})(\sqrt{N\kappa r} + 1)^2 - \kappa r^2 N > 0$. Thus,

$$\Delta_C < 0, \text{ if and only if } R_0 < \frac{1}{(1 + e^{-a})(1 - \frac{1}{\sqrt{N\kappa r}})^2}.$$

In summary, we have proved that

Lemma 4.3. *For* **Type C**, *assume $R_0 > 1$. Then $f_\beta(\beta^*, I^*) > -1$ holds if one of the following conditions is satisfied:*

C-(I): $R_0 < \frac{1}{(1+e^{-a})(1-\frac{1}{\sqrt{N\kappa r}})^2}$;

C-(II): $R_0 > \frac{1}{(1+e^{-a})(1-\frac{1}{\sqrt{N\kappa r}})^2}$ and $I^* < I_{G_c}^1$ or $I^* > I_{G_c}^2$, where $I_{G_c}^1$ and $I_{G_c}^2$ are given in (4.38).

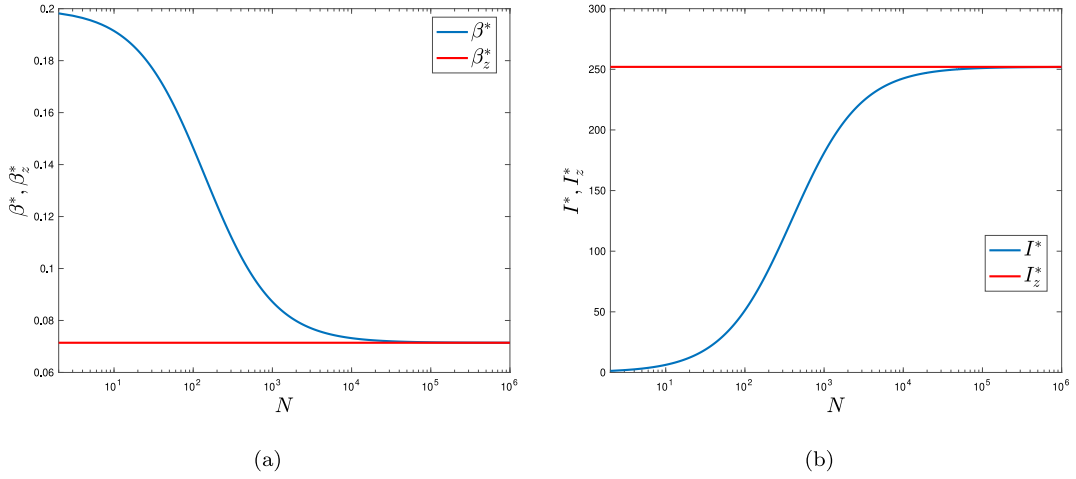

Fig. 3. The curves of endemic states as N vary; (a). β^* of the system (2.3) with the **Type A** and β_z^* of the Zhang–Scarabel–Murty–Wu model (1.1); (b). I^* of (2.3) with the **Type A** and I_z^* of (1.1); values of corresponding parameters are $\beta_c = 0.2$, $r = 1/14$, $\kappa = 0.1$ and then $R_0 = 2.8$.

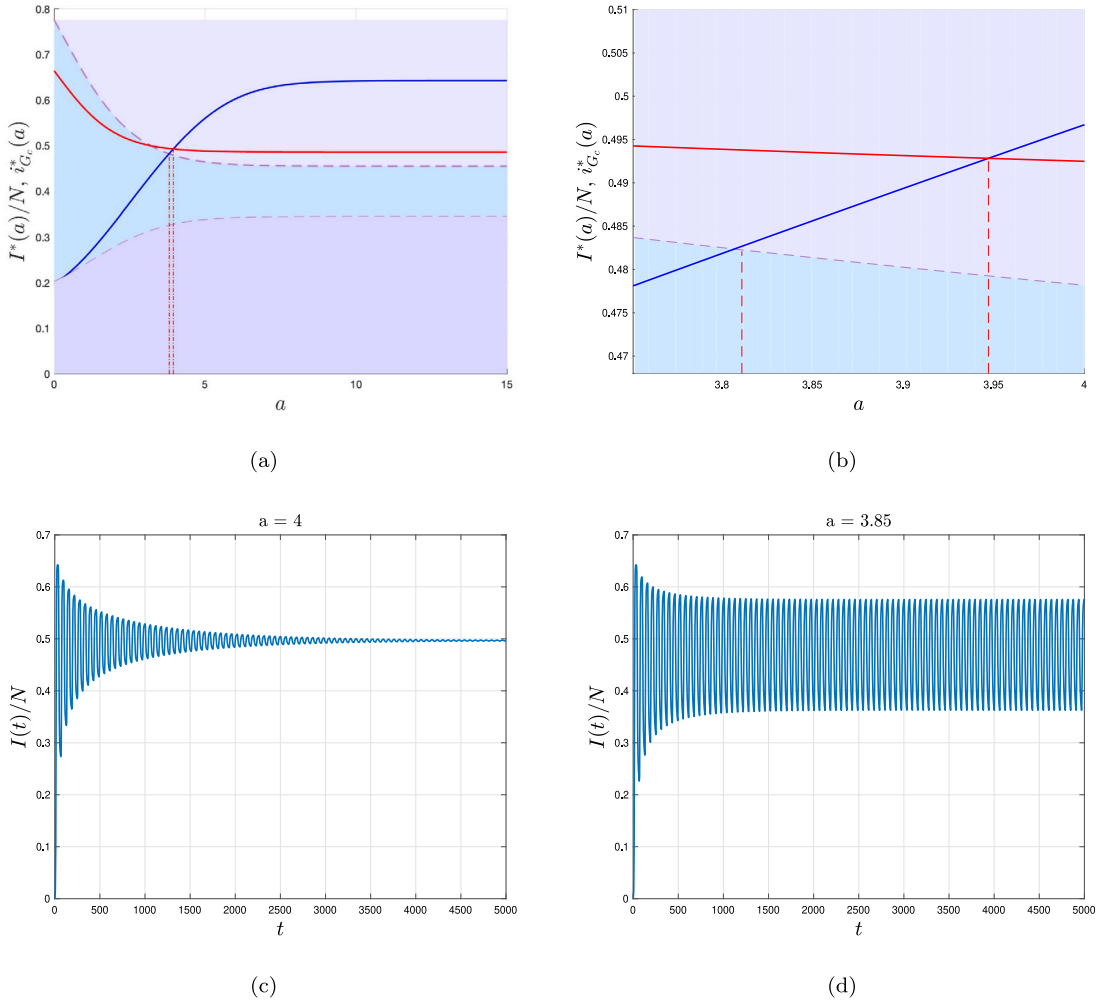

Fig. 4. Some simulations for model (2.3) with **Type C** and $R_0 = 2.8$, (a) The purple-shaded regions represent areas where $y < I^1_{G_c}/N$ or $y > I^2_{G_c}/N$, while the blue-shaded regions give the area where $y \in (I^1_{G_c}/N, I^2_{G_c}/N)$. The blue curve shows the normalized component of endemic equilibrium $I^*(a)/N$, while the red curve represents $i^*_{G_c}(a)$. The critical threshold is $a^* \approx 3.94704$. (b). Zoomed-in view of (a) for the range $a \in [3.75, 4]$. Notice that only when $a > 3.7969$, $I^* > I^2_{G_c}$ holds(i.e. $f'_\beta(\beta^*, I^*) > -1$; (c,d). The proportion of infected individuals $I(t)/N$ with $\tau = 30$. Other parameter values are consistent with those in Fig. 2-(d).

4.2. Birth of oscillatory patterns

Note that for **Type A**, condition $f'_\beta(\beta^*, I^*) > -1$ naturally holds given that $R_0 > 1$. But for **Type B** and **Type C**, it is possible that $f'_\beta(\beta^*, I^*) < -1$ and Fig. 8 shows the existence of a periodic oscillation with $f'_\beta(\beta^*, I^*) < -1$ for **Type B**. We can summarize all discussions so far and use Theorem 3.5 to determine conditions for oscillatory patterns for different types of behavioral functions.

Corollary 4.4. *Assume $R_0 > 1$. We have*

(i) For **Type A**, *when $\kappa > \kappa^*$ (equivalently, $I^*/N < i^*_{c,1}$) where k^* and $i^*_{c,1}$ are given by (4.31) and (4.32), there is a periodic oscillation bifurcated at the EE when τ passes through some critical values. If $\kappa < \kappa^*$ (i.e. $I^*/N > i^*_{c,1}$), no Hopf bifurcation occurs (See Figs. 5 and 6).*

(ii) For **Type B**, *given that $I^* < 1/(\kappa r)$ (ensuring $L_c > 0$), when $I^*/N < i^*_{c2}$, there is a periodic oscillation bifurcated from EE when τ pass through some critical values; when $i^*_{c2} < I^*/N$, no Hopf bifurcation occurs, where $i^*_{c,2}$ is given by (4.34) (See Fig. 7).*

(iii) For **Type C**, *either C-(I) or C-(II) shown in Lemma. 4.3 is met (ensuring $L_c > 0$) when $I^*/N < i^*_{G_c}$. When $I^*/N < i^*_{G_c}$ is satisfied, there is periodic oscillation bifurcated from EE when τ pass through some critical values; when $I^*/N > i^*_{G_c}$, no Hopf bifurcation occurs. (See Fig. 4).*

We can detail comparisons between the Zhang–Scarabel–Murty–Wu model (1.1) and our model as follows:

Remark 4.5 (*Comparison of Conditions for Oscillatory Patterns between During and Post Acute Phase*).. In this remark, we will always assume $R_0 > 1$, so the disease will spread without any behavioral change.

(i) First of all, recall that during the acute phase, the work [1] concluded that conditions for the occurrence of a Hopf bifurcation rely on R_0, independent of the index κ and the endemic level I^*. For any $\kappa > 0$, as long as τ is sufficiently large and passes through some critical value τ^*, a Hopf bifurcation occurs, and an oscillatory pattern emerges around E^*. However, post the acute phase, our result 3.9 shows that occurrence of oscillation is related to the endemic level I^*/N, which is strictly decreasing as κ increases: smaller I^*/N (i.e. $< i^*_g$) or greater κ is more likely to cause the oscillation around E^*. So, in comparison with *Theorem 1* in [1], we need to establish results 4.4-(i) to identify the critical threshold κ^* of κ for a Hopf bifurcation to take place. When $\kappa < \kappa^*$, E^* is always stable for any $\tau \geq 0$. See Fig. 5-(c), 6-(a), where $\kappa < \kappa^* \approx 0.0022$, E^* is stable for all $\tau \geq 0$.

(ii) From the expression (4.31) of κ^*, we see that $\lim_{N\to\infty} k^* = 0$. This means that when N is relatively large, the condition for Hopf bifurcation in Corollary 4.4-(i) coincides with the one in *Theorem 1* in [1], i.e. $R_0 > 1$.

(iii) The threshold τ^* for delay τ during the acute phase obtained in the work [1] is only dependent on R_0, and is a decreasing function of R_0. While the corresponding threshold τ_0 for our model (2.3) post the acute phase is much more involved, it depends not only on R_0. but can also decreases as κ increases (see Fig. 5-(c) that shows τ_0 decreases as κ increases).

4.3. Some additional simulations

We now present some additional numerical results to illustrate the onset of Hopf bifurcations. For comparison with the results in [1] during the acute phase of a pandemic, we use the same parameter values as those specified in [1]. The chosen parameters are displayed in the corresponding figures.

We summarize below the observations from the simulations for **Type A**, illustrated in Figs. 5 and 6.

- Fig. 5-(a) illustrates the results in Corollary 4.4-(i): If $\kappa > \kappa^*$, as τ increases from 0 to pass through τ_0, E^* loses its stability. As τ increases from τ_0, the gap between the maximum and minimum of the periodic fluctuations of infected individuals (normalized by the total population) widens, with the maximum close to 0.7 and the minimum dropping toward near 0.
- Fig. 5-(c) shows that when $\tau < \tau_0$ or $k < k^*$, EE is always stable: When the index κ and delay τ exceed critical values (k^* and τ_0 respectively), oscillatory patterns emerge. Additionally, the threshold τ_0 is decreasing as k^* increases.
- From Fig. 6-(b), the maximum amplitude of the infected population $I(t)$ can exceed $0.6N$ with endemic level $I^*/N < 0.4$ (see Fig. 6-(a)), while the minimum can fall near 0. The amplitude becomes larger and larger as the lag τ increases. Although the lag parameter does not impact the value of I^*, larger τ can enlarge the period and amplify the amplitudes.
- From Fig. 5-(b) and 6-(c), large k decreases the endemic level I^*/N, but leads to an oscillatory wave with the peak of oscillation $I(t)/N$ much greater than I^*/N. Further, comparing the periods of $I(t)/N$ shown in Fig. 6-(c), we observe that k has less impact on periods than the lag τ does. As shown in Fig. 6-(c), κ changes from 0.25^{-4} to 0.05, indicating a significant change in magnitude, while the minimal period slightly increases from 49.4 to 51.8. In contrast, as τ changes from 20 to 90, the minimal period rises substantially from 51.8 to 230.5, see Fig. 6-(b).

The simulations for **Type B** summarized in Fig. 7 confirm Corollary 4.4-(ii). From Fig. 7-(c,d), increment of τ amplifies the amplitude and increases the minimal period of the oscillations bifurcated from E^*. However, there is no established method or technique for a qualitative analysis of the model with $|f'(\beta^*, I^*)| > 1$, Fig. 8 shows numerically the existence of stable periodic solutions.

4.4. Inner-wave distance post the acute phase

We now discuss the inner-wave distance and its ratio to the time lag, expressed as T/τ. By inducing the transform $X(t) = I(t\tau)$ and $Y(t) = \beta(t\tau)$, we obtain the normalized form of the system (2.3):

$$\begin{cases} \frac{dX}{dt} = \tau(Y(t)(N - X(t))/N - r)X(t), \\ Y(t) = f(Y(t-1), X(t-1)). \end{cases} \tag{4.39}$$

The period of the periodic solution of (2.3) is $T_0 := \frac{2\pi}{\omega_0}$ and the corresponding period of the periodic solution of (4.39) is $T'_0 := \frac{2\pi}{\tau_k\omega_0}$. From (3.19), we know

$$\frac{\pi}{2} < \omega_0\tau_0 < \pi, \quad 2\pi < \omega_0\tau_k < (2k+1)\pi, \ k \geq 1.$$

Therefore,

$$2 < \frac{2\pi}{\omega_0\tau_0} < 4, \quad \frac{1}{k+1} < \frac{2\pi}{\omega_0\tau_k} < 1, \ k \geq 1,$$

and

$$\tau_k > \frac{2\pi}{\omega_0}, \ k = 1, 2, \ldots$$

Then for $\tau > \tau_k$, there exists an integer n such that $\tau/n < T_0 < \tau$. That means periodic solutions of (4.39) (or (2.3)) on the first Hopf branch based at τ_0 have periods bounded between 2 and 4 (or 2τ and 4τ), and thus are "slowly oscillating". Meanwhile, periodic solutions on other Hopf branches have periods smaller than 1 (or τ) and thus are "fast oscillating". From Fig. 5-(a), 6-(b) and 7-(d), we observe that bifurcating periodic solutions may continue to exist even for large values of τ, numerically indicating the possibility of global continuations of the local Hopf bifurcation given in Theorem 3.5.

Numerical simulations given in Fig. 9 also show that delay-induced transient oscillations can exist for the system (4.39), consequently for the system (2.3). The fast oscillating periodic solutions on the kth

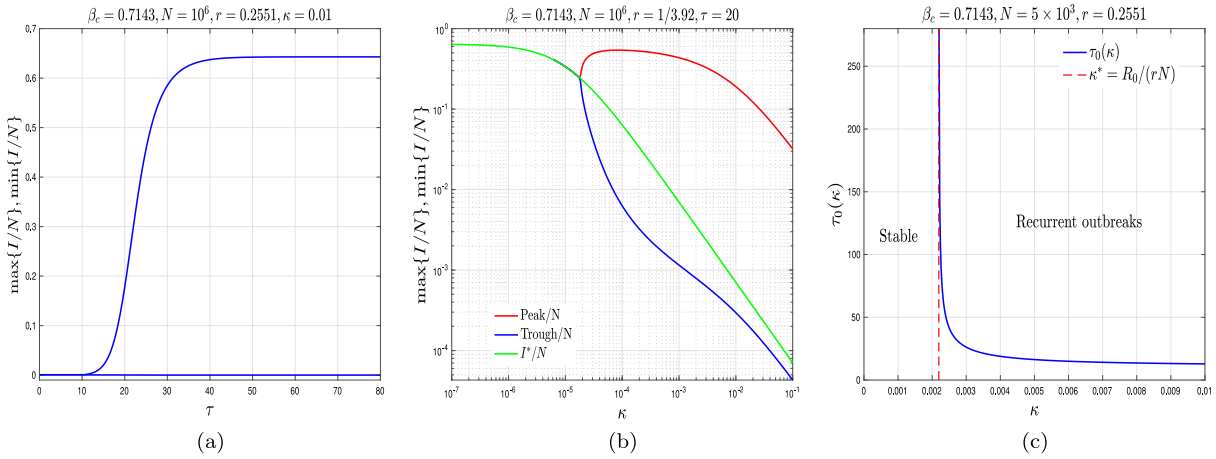

Fig. 5. The bifurcation diagram for model (2.3) with **Type A** and $R_0 = 2.8$, $(\beta^*, I^*) = (0.2553, 704.848)$. (a). The bifurcation diagram about τ with $\tau_0 \approx 10.61$; (b). The bifurcation diagram about κ with $\kappa^* \approx 1.1^{-5}$; (c). The Hopf bifurcation curves $\tau_0(\kappa)$ in the $\kappa - \tau_0$ parameter space with $\kappa^* \approx 0.0022$.

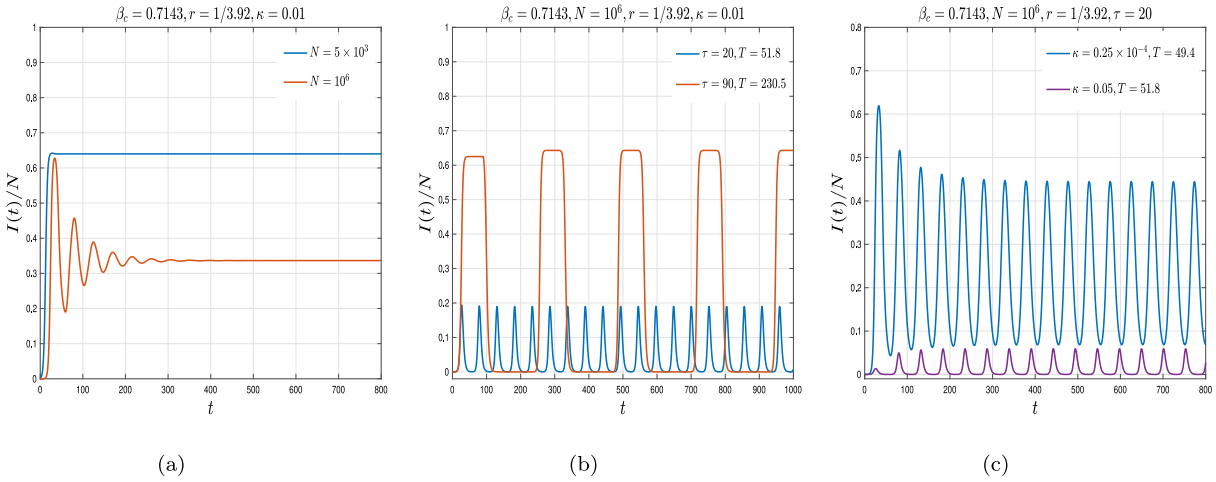

Fig. 6. An illustration of the proportion of infected individuals $I(t)/N$ for (2.3) with **Type A**.

branch for $k \geq 1$ are unstable and quickly converge to a slowly oscillating periodic solution.

Fig. 10 illustrates the ratio of the (minimal) period T to the lag τ is bounded within a particular range (i.g. $[2, q_M]$). However, the qualitative behaviors of T/τ concerning τ depend on the choice of $F(\xi)$. In applications to public health, the ratio of T/τ is essential for predicting the inner-wave duration; mathematically, estimating this ratio plays a crucial role in proving the global continuation of Hopf bifurcations. A lower ratio means the response time is too long, while a higher ratio means either the response is effective or the inner-wave duration is sufficiently long.

5. Discussion and future work

In this paper, we studied the transmission dynamics of an emerging infectious disease post its acute phase of the global pandemic, and we used a system of an epidemic SIS model coupled with an algebraic equation for behavioral adaptation. We first showed how the equilibrium state for both infection transmission and disease transmission effective contact is determined by the basic epidemic characteristics, such as the basic reproduction number, and by the population's behavioral response to perceived risks (such as hospitalization rate and ICU admission), and then showed how the risk perception delay and community's behavioral change delay destabilize the equilibrium state, leading to nonlinear periodic waves in both transmission dynamics and effective contacts. We further established the estimation of the duration from peak to peak of the periodic waves using risk perception and behavioral change delay. We believe this study provides some qualitative insights for possible scenarios of an emerging infectious disease when it enters its so-called endemicity–the post acute phase of the pandemic.

The work is based on the early study [1] that was designed to explain mechanisms behind widely observed multi-waves during the acute phase of the COVID-19 pandemic. Compared with some of the results in this early study, our results for the post acute phase show that human behavioral adaptation to perceived risks cannot induce periodic oscillations (or sustained waves) if the equilibrium state is so large (larger than half of the population) that the saturation effect of infected populations becomes more dominated than any human adaptive behaviors. We also showed that when the endemic level is relatively low, the periodic oscillation through the Hopf bifurcation mechanism can fluctuate with larger amplitude so that its peak value can be very large while its lowest value (of infected individuals) can be close to zero, so decision-makers must avoid miscommunication of the effectiveness of any public health interventions (at the valley of disease transmission) and prepare the healthcare system for a large number of infections at the peak time. The duration between two peaks is closely linked to the period of the periodic waves, and our study shows that the community's flexibility index κ (for behavioral change) has less

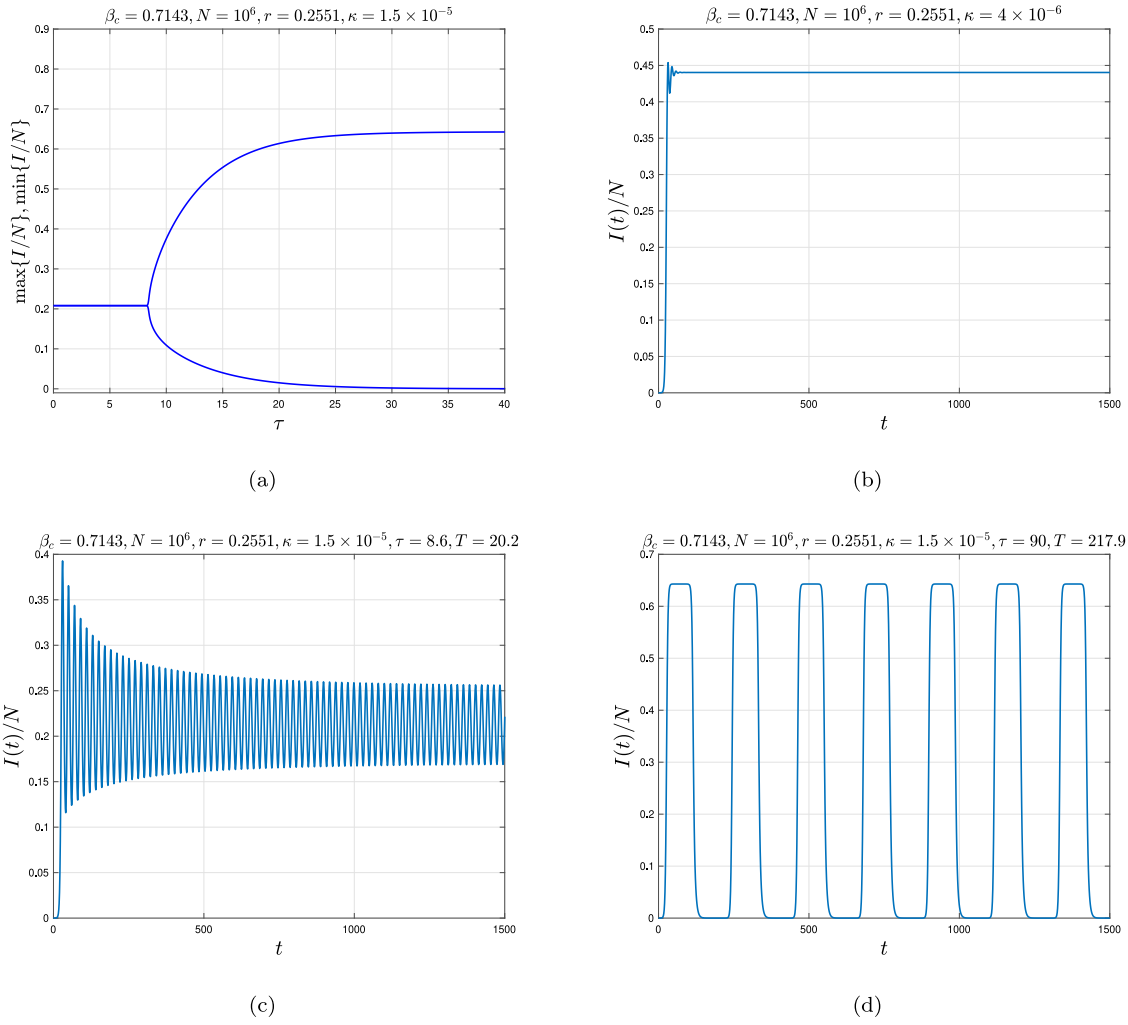

Fig. 7. Some simulations for **Type B** with $|f'_{\beta}(\beta^*, I^*)| < 1$. (a). The bifurcation diagram about τ with $\tau_0 \approx 8.43$; (b,c,d). The proportion of infected individuals $I(t)/N$. For (b), $(\beta^*, I^*) = (0.322, 208103.58)$, and $I^*/N = 0.4403 > i^*_{c2} \approx 0.02$; For (c,d), $(\beta^*, I^*) = (0.456, 440299.77)$, and $I^*/N = 0.2081 < 1/(\kappa N r) \approx 0.261 < i^*_{c2}$.

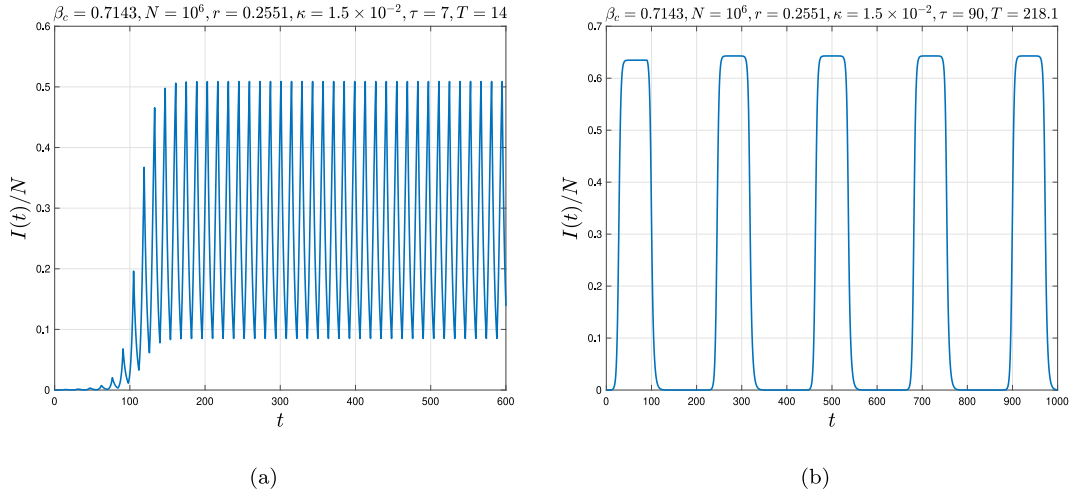

Fig. 8. The solution for **Type B** with $|f'_{\beta}(\beta^*, I^*)| > 1$.

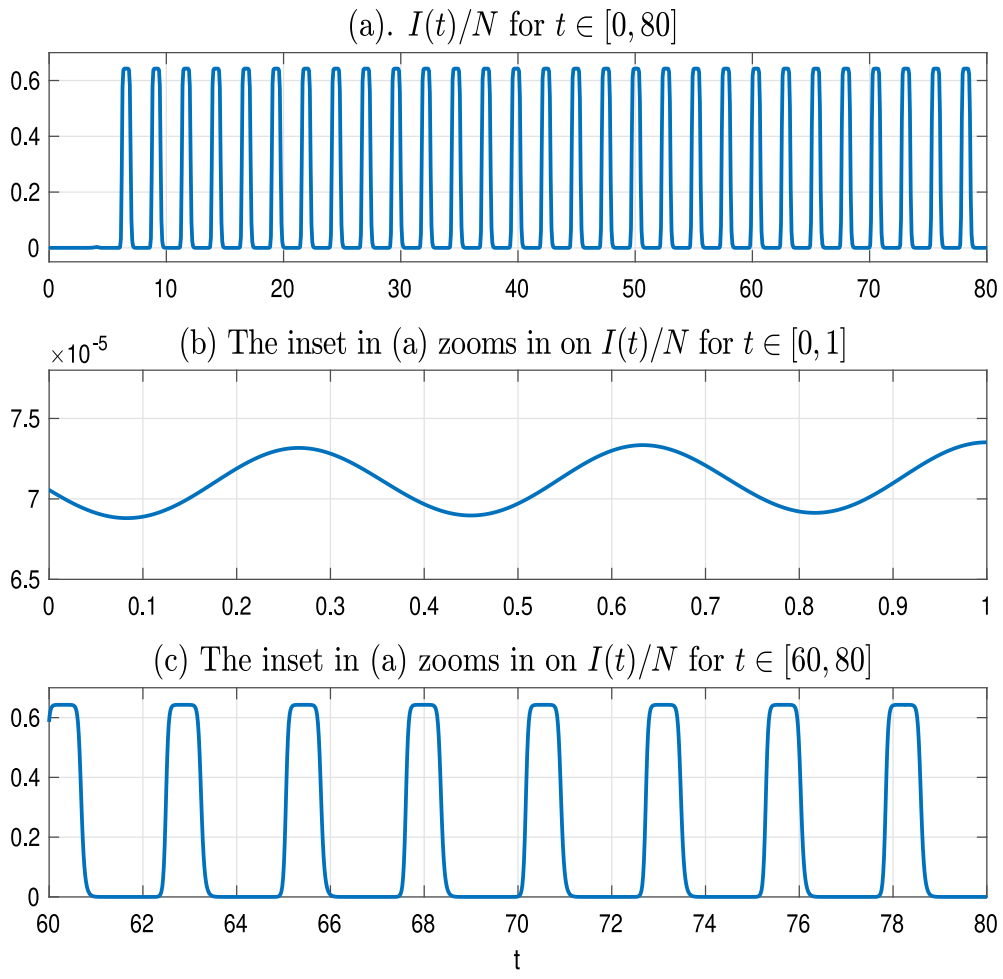

Fig. 9. A solution of the normalized system (4.39) with **Type B** first approaches a fast oscillating unstable periodic solution with the minimal period closed to 0.3617 before it converges to the slowly oscillating stable periodic solution with the minimal period closed to 2.5613. $\tau = 90$, $\kappa = 0.005$ and other parameter values are the same as in Fig. 7.

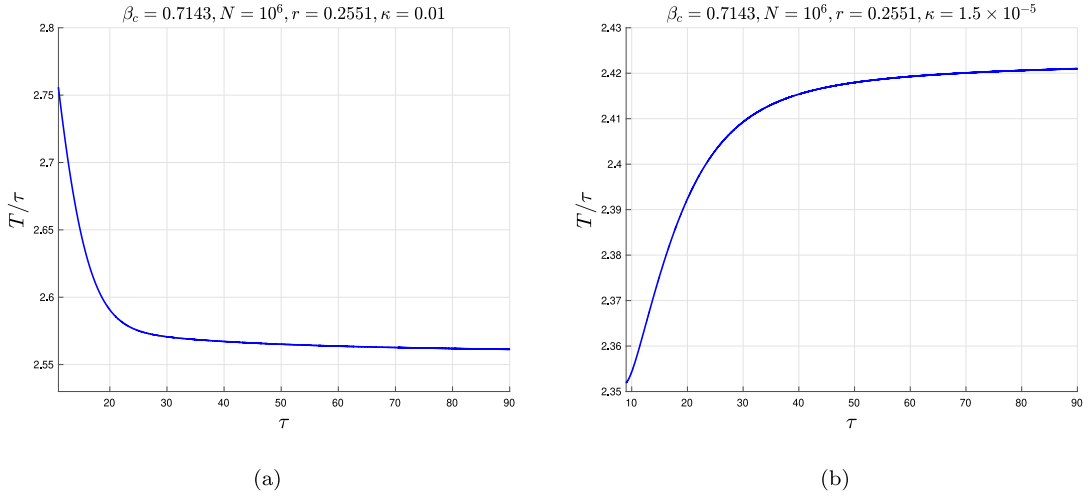

Fig. 10. Ratio of period/delay for the periodic solutions of (2.3) concerning τ. (a). For **Type A**. (b). For the **Type B** with $|f'_{\beta}(\beta^*, I^*)| < 1$.

impact on the inter-peak duration than the community's effectiveness to implement the desired behavioral response to perceived risks. A higher index κ reduces the level of endemics, but when the delay is large, an additional increase in κ can generate an oscillation in the level of infections in the population with a peak value much higher than the equilibrium state I^*.

There are several important questions remaining for further studies. First of all, we focused on the local Hopf bifurcations when the delay passes through the calculated critical values. How this local Hopf bifurcation of periodic solutions behavior when the delay is away from these critical values requires in-depth global Hopf bifurcation analyses. Also, the theoretical foundation for local Hopf bifurcation of our coupled system, regarded as a special form of neutral functional differential equations, requires that the associated operator related to the "neutral part" to be stable. Namely, we require that $|f'_{\beta}(\beta^*, I^*)| < 1$, though our numerical simulations suggest Hopf bifurcation of periodic solutions do take place when $|f'_{\beta}(\beta^*, I^*)| > 1$ and when τ is relatively small, see Fig. 8. This provides a good example to motivate the development of the qualitative theory for neutral functional differential equations with unstable neutral operators.

There have been important studies on periodic recurrence of emerging and reemerging diseases by incorporating seasonal variations of disease transmission effective contacts [13–16]. There have also been intensive efforts in modeling and understanding the impact of behavioral changes on disease transmission dynamics, see, for example, [1, 17–21] and references therein. Our work aims to incorporate risk perception and behavioral adaptation to perceived risks in a simple mechanistic model involving two fundamental actionable parameters (the population flexibility κ, and the population's response delay τ) to provide a scenario analysis of the equilibrium state and possibility of periodic oscillations in order to inform decision making and behavioral changes for better prevention and control of emerging infectious diseases post the acute phase of a pandemic.

CRediT authorship contribution statement

Tianyu Cheng: Writing – review & editing, Writing – original draft, Visualization, Validation, Software, Methodology, Investigation, Funding acquisition, Formal analysis, Conceptualization. **Jianhong Wu:** Writing – review & editing, Writing – original draft, Validation, Supervision, Project administration, Methodology, Investigation, Funding acquisition, Formal analysis, Conceptualization.

Declaration of competing interest

The authors declare no conflicts of interest.

Acknowledgments

The work has been supported by the NSERC-Sanofi Industrial Research Chair program "Vaccine Mathematics, Modelling and Manufacturing" (517504), and the Discovery Grant of the Natural Science and Engineering Research Council of Canada (105588).

Data availability

Data will be made available on request.

References

[1] X. Zhang, F. Scarabel, K. Murty, J. Wu, Renewal equations for delayed population behaviour adaptation coupled with disease transmission dynamics: A mechanism for multiple waves of emerging infections, Math. Biosci. 365 (2023) 109068.
[2] World Health Organization, COVID-19 updates, 2024, https://www.who.int.
[3] United Nations News, COVID-19 making worrying comeback, WHO warns, amid summertime surge, 2024, https://news.un.org/en/story/2024/08/1152866.
[4] Centers for Disease Control, Prevention, COVID-19 data tracker: Recent trends and updates, 2024, https://www.cdc.gov/covid-data-tracker.
[5] T. Ulrichs, M. Rolland, J. Wu, M.C. Nunes, C. El Guerche-Séblain, A. Chit, Changing epidemiology of COVID-19: potential future impact on vaccines and vaccination strategies, Expert. Rev. Vaccines 23 (1) (2024) 510–522.
[6] H. McCallum, N. Barlow, J. Hone, How should pathogen transmission be modelled? Trends Ecol. Evol. 16 (6) (2001) 295–300.
[7] J.M. Epstein, J. Parker, D. Cummings, R.A. Hammond, Coupled contagion dynamics of fear and disease: mathematical and computational explorations, PLoS One 3 (12) (2008) e3955.
[8] Pengfei Song, Jianhong Wu, Yanni Xiao, Modelling the effect of human heterogeneity on infectious disease transmission dynamics, 2024.
[9] Shuangshuang Yin, Jianhong Wu, Pengfei Song, Optimal control by deep learning techniques and its applications on epidemic models, J. Math. Biol. 86 (3) (2023) 36.
[10] O. Diekmann, S.A. van Gils, S.M. Verduyn Lunel, H.-O. Walther, Delay Equations, Functional-, Complex-, and Nonlinear Analysis, vol. 110, Springer Science & Business Media, 2012.
[11] B.D. Hassard, N.D. Kazarinoff, Y.H. Wan, Theory and applications of Hopf bifurcation, J. Stat. Mech. Theory Exp. 41 (1981).
[12] John Von Neumann, Oskar Morgenstern, Theory of games and economic behavior: 60th anniversary commemorative edition, in: Theory of Games and Economic Behavior, Princeton University Press, 2007.
[13] I.B. Schwartz, Small amplitude, long period outbreaks in seasonally driven epidemics, J. Math. Biol. 30 (1992) 473–491.
[14] A.L. Bertozzi, E. Franco, M.B. Mohler, D. Sledge, The challenges of modeling and forecasting the spread of COVID-19, Proc. Natl. Acad. Sci. USA 117 (29) (2020) 16732–16738.
[15] K. Dietz, The incidence of infectious diseases under the influence of seasonal fluctuations, in: Mathematical Models in Medicine: Workshop, Mainz, March 1976, vol. 76, Springer Berlin Heidelberg, 1976, pp. 1–15.
[16] S. Sobolevsky, R. Campari, Recurrent outbreaks of measles, chickenpox and mumps: I. Seasonal variation in contact rates, Am. J. Epidemiol. 98 (6) (1973) 453–468.
[17] T. Cheng, X. Zou, Modelling the impact of precaution on disease dynamics and its evolution, J. Math. Biol. 89 (1) (2024) 1.
[18] H. Berestycki, B. Desjardins, B. Heintz, J.M. Oury, Plateaus, rebounds and the effects of individual behaviours in epidemics, Sci. Rep. 11 (1) (2021) 18339.
[19] S. Funk, M. Salatha, V.A. Jansen, Modelling the influence of human behaviour on the spread of infectious diseases: a review, J. R. Soc. Interface 7 (50) (2010) 1247–1256.
[20] B. Morsky, F. Magpantay, T. Day, E. Akcay, The impact of threshold decision mechanism of collective behaviour on disease spread, Proc. Natl. Acad. Sci. USA 120 (19) (2023) e2221479120.
[21] P. Manfredi, A. D'Onofrio, Modelling the Interplay Between Human Behaviour and the Spread of Infectious Diseases, Springer Science Business Media, 2013.